Measurement of contact resistivity at metal-tin sulfide (SnS) interfaces

Chuanxi Yang, Leizhi Sun, Riley E. Brandt, Sang Bok Kim, Xizhu Zhao, Jun Feng, Tonio Buonassisi, and Roy G. Gordon

Citation: Journal of Applied Physics **122**, 045303 (2017); doi: 10.1063/1.4992086
View online: http://dx.doi.org/10.1063/1.4992086
View Table of Contents: http://aip.scitation.org/toc/jap/122/4
Published by the American Institute of Physics

Measurement of contact resistivity at metal-tin sulfide (SnS) interfaces

Chuanxi Yang,[1,a)] Leizhi Sun,[1,a)] Riley E. Brandt,[2] Sang Bok Kim,[1] Xizhu Zhao,[1] Jun Feng,[1] Tonio Buonassisi,[2] and Roy G. Gordon[1,b)]
[1]*Harvard University, Cambridge, Massachusetts 02138, USA*
[2]*Massachusetts Institute of Technology, Cambridge, Massachusetts 02139, USA*

(Received 5 April 2017; accepted 25 June 2017; published online 25 July 2017)

We measured the contact resistivity between tin(II) sulfide (SnS) thin films and three different metals (Au, Mo, and Ti) using a transmission line method (TLM). The contact resistance increases in the order Au < Mo < Ti. The contact resistances for Au and Mo are low enough so that they do not significantly decrease the efficiency of solar cells based on SnS as an absorber. On the other hand, the contact resistance of Ti to SnS is sufficiently high that it would decrease the efficiency of a SnS solar cell using Ti as a back contact metal. We further estimate the barrier heights of the junctions between these metals and tin sulfide using temperature-dependent TLM measurements. The barrier heights of these three metals lie in a narrow range of 0.23–0.26 eV, despite their large differences in work function. This Fermi level pinning effect is consistent with the large dielectric constant of SnS, and comparable to Fermi-level pinning on Si. The contact resistivity between annealed SnS films and Mo substrates under light illumination is as low as 0.1 $\Omega\,cm^2$. *Published by AIP Publishing.* [http://dx.doi.org/10.1063/1.4992086]

I. INTRODUCTION

Tin(II) sulfide (SnS) has recently been demonstrated as a promising material for solar cells.[1,2] Tin and sulfur are both Earth-abundant and non-toxic, whereas other thin film solar cells often require toxic elements such as cadmium, selenium, tellurium, or lead, or rare metals such as indium or silver. SnS has a direct band gap of 1.3 eV and an indirect band gap of 1.1 eV, which are nearly ideal for solar cell absorbers.[3–5] It has native *p*-type conduction due to the small enthalpy of formation of tin vacancies, which generate shallow acceptors.[4,6] SnS has a high absorption coefficient ($\alpha > 10^4\,cm^{-1}$), so SnS layers less than 500 nm thick can absorb 75% of the solar spectrum above the direct band gap. Another beneficial trait of SnS is its stability in the presence of atmospheric water and oxygen, as the oxidation of SnS yields a thin, dense, and stable tin oxide layer on the surface that inhibits further oxidation. Recent studies show that this thin oxide layer can passivate the SnS/buffer layer interface, which leads to improved solar cell efficiency.[1,2,5,7]

To minimize the series resistance and improve the performance of SnS solar cells, it is important to understand the electrical properties of the interface between SnS and contact metals. SnS is a *p*-type semiconductor with a high ionization potential. Thus, high work-function metals are expected to form low-resistance, ohmic contacts with SnS.

Gold (Au), with its high work function, would be expected to provide low-resistance contact to p-type semiconductors, such as SnS. In addition, Au is highly reflective in the infrared, so as a back contact it should reflect transmitted photons back through the absorber for a second chance to be absorbed. Thus, thinner absorber layers could be used with Au back contacts. However, Au is a rapid diffuser during annealing, so it is not suitable as a back contact for cells grown on an Au back contact as a substrate.

Molybdenum (Mo) has a moderate, but not high, work function, between 4.36 and 4.95 eV.[8] Nevertheless, Mo forms fairly low-resistance interfaces with p-type absorber materials and has a low electrical resistivity of 5.3×10^{-6} Ω cm at 300 K.[9] Mo is the most common choice of back contact metal for a wide range of thin film solar cells, including cadmium telluride (CdTe), copper indium gallium sulfide selenide (CIGS), copper zinc tin sulfide selenide (CZTS), and tin sulfide (SnS) solar cells.[10] Because of its high melting point and strong metal bonding, Mo may not diffuse into other layers of solar cells even during annealing at elevated temperatures.[6] This property means that Mo as a back contact material is compatible with either superstrate or substrate configurations. Furthermore, sputtering Mo under a certain condition achieves strong adhesion to substrates such as glass or silica, followed by sputtering under other conditions to form a low resistivity contact metal (as a layer that contacts the absorber).[11]

Titanium (Ti) is commonly used as a contact to silicon semiconductors, to which it provides strong adhesion. However, Ti has a low work function, so that it might be expected to have a high contact resistance with p-type semiconductors such as SnS. Nevertheless, such simple predictions do not take into account pinning by interfacial states and reactions at the interface, so Ti was included in our study of contact resistance.

In this study, contact resistivities between SnS and the metals Mo, Au, and Ti were systematically investigated using the transmission line method (TLM). Both Mo and Au were found to form ohmic contacts to SnS with low contact resistance, while Ti has a somewhat higher contact resistance. This information should help to improve further the performance of SnS solar cells.

[a)]C. Yang and L. Sun contributed equally to this work.
[b)]Author to whom correspondence should be addressed: gordon@chemistry.harvard.edu

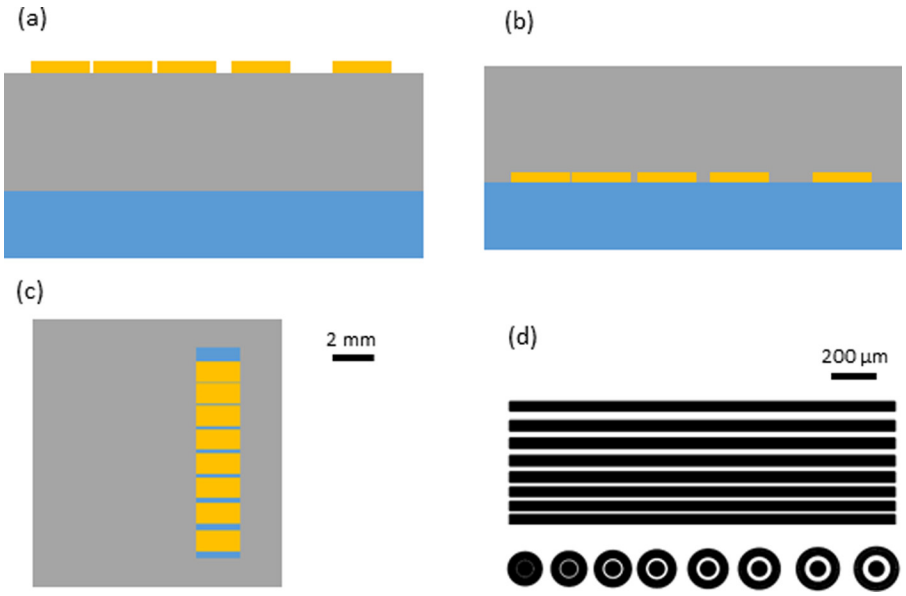

FIG. 1. Cross-sectional schematic diagram of (a) superstrate and (b) substrate test structures (not to scale). Yellow parts refer to 100 nm thick metal patterns; grey parts are SnS material (500 nm thick); blue parts are thermal oxide substrates. (c) Top-view of substrate-based structure. A rectangular window is etched through the grey SnS layer to enable probing the linear metal lines. Only linear TLM pattern is applied in this configuration (not to scale). (d) Linear (top) and circular (bottom) TLM patterns used in the superstrate test structure.

II. EXPERIMENTS

SnS films were grown in a custom-built hot-wall atomic layer deposition (ALD) reactor at a deposition temperature of 200 °C in a closed valve mode. The precursors used were bis(*N*,*N*′-diisopropylacetamidinato) tin(II) and hydrogen sulfide (H_2S). More details of the film growth conditions can be found elsewhere.[12]

TLM patterns were fabricated in two configurations: "superstrate" cells with metal contacts grown on top of the SnS film [Fig. 1(a)] or "substrate" cells with SnS grown on top of the metal back contact [Fig. 1(b)]. To model the contacts in a superstrate cell, blanket SnS films 500 nm thick were grown on SiO_2 substrates, and 100 nm thick metal contact patterns of both linear TLM (LTLM) and circular TLM patterns (CTLM) were deposited on top using electron beam evaporation, as in Fig. 1(d). The fabrication process of this structure is similar to the way in which superstrate solar cells are made.

Using the superstrate configuration, we obtained the contact resistance (ρ_c) and sheet resistance (R_{sh}) of SnS by plotting R_t vs. d (LTLM), or R_t vs. $\ln(R/r)/2\pi$ (CTLM), as shown in Fig. 2. For LTLM[13,14]

$$R_t = R_{sh}\left(\frac{d}{W}\right) + \frac{2\sqrt{\rho_c R_{sh}}}{W}, \tag{1}$$

where R_t is the total resistance, d is the gap width between adjacent contacts (from 5 μm to 50 μm, with a step of 5 μm), ρ_c is specific contact resistivity in $\Omega\cdot cm^2$, and W is the width of contacts, equal to 50 μm. The sheet resistance of the SnS is proportional to the slope of the line, whereas contact resistivity is found from the intercept of the line with the y axis.

For CTLM[15]

$$R_t = R_{sh}\left[\frac{\ln\left(\frac{R}{r}\right)}{2\pi}\right] + \frac{\sqrt{\rho_c R_{sh}}}{2\pi}\left(\frac{1}{R}+\frac{1}{r}\right), \tag{2}$$

where r and R denote the radii of the central dot (50 μm) and the outer ring (from 55 μm to 100 μm, with a step of 5 μm), respectively. R_{sh} and ρ_c are obtained from non-linear least-squares fitting of this equation.

In order to understand better the contact potential barrier and carrier transport mechanism at the metal-on-SnS junction, temperature-dependent current-voltage (*I*-*V*) measurement of the CTLM patterns were also carried out in the range of 225–425 K. The barrier heights (ϕ_B) between the p-type SnS and different metals were estimated by fitting the contact resistivity values to the equation: $\rho_C = \rho_0 \exp(q\phi_B/kT)$, where ϕ_B and ρ_0 are constants fitted separately for each metal.[14]

The substrate structure, in which the SnS films were grown on top of the metal TLM patterns, followed the same fabrication approach in which our current SnS-based solar cells are grown on a back metal contact of molybdenum.[12]

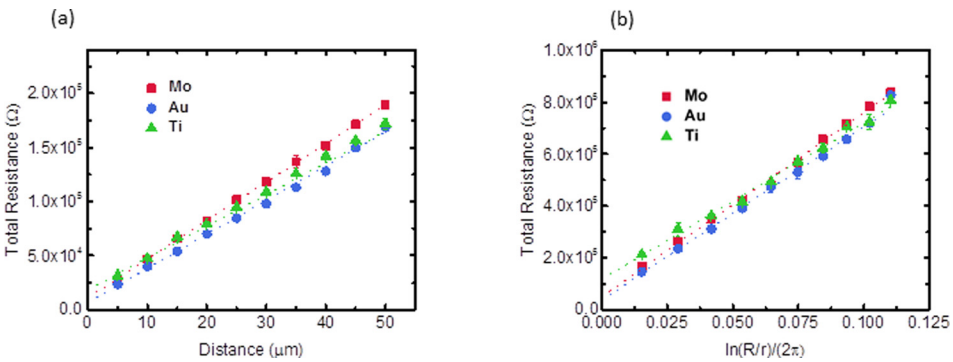

FIG. 2. Measured resistance vs. spacing for (a) linear and (b) circular TLM patterns in the superstrate configuration at room temperature.

TABLE I. Comparison of metal work function, SnS sheet resistance, and specific contact resistivities of various metals on SnS determined by CTLM and LTLM methods in both superstrate and substrate configuration.

Metal	Φ (eV)	Method	R_{sh} (Ω/sq)	ρ_c (Ω·cm^2)	$\varnothing_B$ (eV)
Superstrate configuration					
Au	5.1–5.47	CTLM	$(6.66 \pm 0.08) \times 10^6$	0.057 ± 0.018	0.23
		LTLM	$(6.31 \pm 0.13) \times 10^6$	0.073 ± 0.042	
Mo	4.36–4.95	CTLM	$(7.09 \pm 0.08) \times 10^6$	0.09 ± 0.02	0.24
		LTLM	$(7.13 \pm 0.05) \times 10^6$	0.18 ± 0.02	
Ti	4.33	CTLM	$(6.03 \pm 0.19) \times 10^6$	0.57 ± 0.12	0.26
		LTLM	$(5.85 \pm 0.05) \times 10^6$	0.61 ± 0.05	
Substrate configuration					
Au	5.1–5.47	LTLM	$(3.86 \pm 0.03) \times 10^6$	0.22 ± 0.05	N/A
Mo	4.36–4.95	LTLM	$(1.01 \pm 0.01) \times 10^7$	0.87 ± 0.23	
Ti	4.33	LTLM	$(8.94 \pm 0.03) \times 10^6$	2.7 ± 0.24	

The linear TLM patterns used are similar to those in the superstrate structure. The width of the contact (W) is 1 mm, and the gaps between adjacent contacts (d) are 20 μm, 40 μm, 60 μm, 80 μm, 100 μm, 200 μm, and 300 μm [Fig. 1(c)]. After metal patterns were electron beam evaporated onto SiO_2, a 500 nm SnS film was grown on top. It should be noted that due to inevitable air exposure of the metals between processing steps, a thin metal oxide layer likely exists at the Ti/SnS and Mo/SnS interfaces. To contact these metal pads electrically, the film was patterned with photolithography and etched in a dilute HCl solution; see Fig. 1(c). After an initial current-voltage measurement of these samples, they were annealed at 400 °C in an H_2S (10 Torr, 99.5% in N_2) environment for 1 h.[1,12] The same measurement was repeated both in the dark and under 100 mW cm^{-2} AM 1.5 illumination through the SnS layer.

III. RESULTS AND DISCUSSION

I-V measurements showed that Au, Mo and Ti formed ohmic contacts with SnS, which is consistent with earlier findings.[16] The results of sheet resistance and contact resistivity measurements are summarized in Table I. Both CTLM and LTLM yield similar trends, indicating the robustness of both methods. Au has the lowest specific contact resistivity among all the metals investigated, and Mo is only slightly higher than Au. The specific contact resistivity of Ti with SnS is one order of magnitude higher than Au or Mo, making it less preferable as a back contact metal in SnS-based solar cells. Contact resistivity values measured by the CTLM are generally lower than those measured by the LTLM. This discrepancy could be caused by the edge current present in the LTLM methods, which error is eliminated in the CTLM.[17]

As expected, the low contact resistivity of Au can be explained by its high work function in the range of 5.1–5.47 eV,[8] and its ability to dope SnS p-type. However, Mo also has a low contact resistance similar to Au, but this low value cannot be explained by the same two factors as for Au. The work function of Mo is between 4.36 and 4.95 eV,[8] which is not as high as that of SnS, between 4.9 and 5.8 eV.[18] A more likely explanation for the low contact resistance of Mo with SnS is that Mo reacts with sulfur from the SnS to form a MoS_x interlayer, which does have a high work function that favors low resistance,[19] ohmic contact with SnS. Ti has a low work function, around 4.33 eV,[8] which can explain its relatively high contact resistance with SnS. Al and Ag also have relatively low work functions in the range of 4.06–4.26 eV and 4.26–4.74 eV, respectively.[8] Their current-voltage characteristics in metal/SnS/metal structures show nonlinear behavior, indicating the formation of Schottky barriers.

Figure 3 plots the specific contact resistivity as a function of temperature. For temperatures measured above 225 K, ρ_C exhibits an Arrhenius-type dependence on temperature. This indicates that the dominating conduction mechanism is thermionic emission (TE).[20] In this regime, ρ_C increases as temperature decreases and fewer electrons possess sufficient thermal energy to overcome the Schottky barrier at the metal/SnS interface. The barrier heights between the p-type SnS and Au, Mo, and Ti were estimated to be 0.23 eV, 0.24 eV, and 0.26 eV respectively, as presented in Fig. 3(b). The dependence of $\varnothing_B$ on metal work function (Φ_m) is very weak; the slope $S = -\Delta\Phi_B/\Delta\Phi_m$ is only 0.03. This small S value indicates a strong Fermi level pinning effect [see Fig. 3(b), inset], which is even smaller than that reported for Si in the literature.[14,21]

Fermi level pinning effects have been described by a variety of models, including the presence of intrinsic surface states, and metal-induced gap states (MIGS). In the layered crystal structure of SnS, the layer planes are held together by van der Waals forces. A free layer plane surface is expected to be chemically inert, with few surface states,[22] therefore suggesting that intrinsic surface states may not be responsible

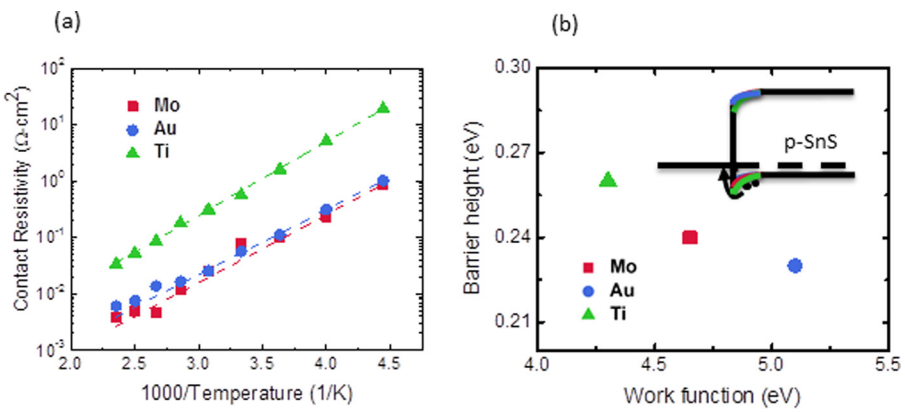

FIG. 3. (a) Specific contact resistivity in the temperature range of 225 K–425 K plotted on a semi-log scale. Dashed lines represent the fits for each metal. (b) Barrier height as a function of metal work function. Inset: schematic band diagram showing the Fermi level pinning effects.

for this pinning. However, recent band offset measurements on SnS suggest that Fermi level pinning may be a major limitation to the efficiency.[23]

In the MIGS model (and related models), the pinning parameter, or slope S was found to be correlated with the electronic part of the dielectric constant, ε_∞, of the semiconductor:[24]

$$(1/S - 1) = 0.1(\varepsilon_\infty - 1)^2. \quad (3)$$

In SnS, ε_∞ has been found to vary as a function of crystallographic orientation, between 11.85 and 14.02.[25] This large ε_∞ would imply an S value of 0.05–0.08, which is not too far from the value, 0.03, obtained in our experiments. This suggests that the high degree of pinning at the metal/SnS interface may be connected to its high charge screening, due to its high dielectric constant.

The results for superstrate configuration provide much information about the specific contact resistivity and carrier transport mechanism between different metals and SnS. Nevertheless, it is not necessarily representative of the back contact resistance in substrate configuration SnS solar cells, in which the metal contact is deposited first. To simulate the substrate case, LTLM metal lines were deposited on SiO_2 substrates and then blanket SnS films were grown by ALD. The substrate configuration can better simulate substrate-based SnS solar cell devices in three ways. First, current SnS solar cells require a post-deposition annealing process in an H_2S environment to promote grain growth.[1] In the superstrate configuration, with metal patterns covering the surface of SnS, the gas environment of the annealing step is changed. Second, considering its highly-anisotropic nature,[26] SnS deposited on a SiO_2 substrate may have a different crystal orientation, and thus different electrical properties, compared to the SnS in a substrate-based solar cells. Third, with no metal features shadowing the SnS, it is possible to carry out *I-V* measurements under illumination, therefore revealing the contribution of back contact resistance to the total series resistance in an operating solar cell.

By using ALD growth, SnS covered the metal contacts conformally, which can be seen in the cross-sectional SEM image of SnS grown near the boundary of Mo and SiO_2 [Fig. S1]. However, since nucleation of ALD SnS depends heavily on the substrate, SnS films grown on different substrates have different crystal orientations, and thus different electrical properties. Figure S2 shows the X-ray diffraction (XRD) spectra of as-deposited and annealed SnS thin films on different substrates. These data show that Mo and Ti substrates induce similar crystallite orientations of the SnS, but on Au substrates SnS grows with quite different orientations of its crystallites.

Specific contact resistivity and sheet resistance of the as-deposited films are shown in Table I and Fig. 4 for comparison with those measured in superstrate configuration. The measured contact resistivity of Mo/SnS and Ti/SnS interfaces in the substrate configuration is higher than those obtained from the superstrate configuration, possibly because of the inevitable existence of a thin metal oxide layer. Another difference is that the sheet resistance of SnS grown on linear Au patterns is only half of that on the other two metals. This may be due to two effects. First, Au has a high diffusivity in many other semiconductors and may create acceptor states that increase the hole concentration of the *p*-type SnS. Second, the film crystallite orientations on Au are different, and higher conductivity in the SnS layer planes may result in a lower sheet resistance. This effect is supported by XRD data of SnS on different metal substrates in Fig. S2.

The ρ_c of both Mo/SnS and Ti/SnS interfaces, and the sheet resistance of SnS, dropped after annealing, as shown in Fig. 4. This is because annealing increases both the hole concentration and mobility of the SnS thin films, as can be seen from the Hall measurement results of SnS before and after annealing (as shown in the supplementary material). Under illumination, photogenerated carriers further bring down ρ_c and R_{sh}. The specific contact resistivity of Mo/SnS under light is as low as about 0.1 Ω cm^2, which contributes around 20% of our current solar cell series resistance;[12] that of Ti/SnS is 0.36 Ω cm^2. In the latter case, 0.36 Ω cm^2 can lead to a 0.1% absolute efficiency loss in current SnS solar cells with 4.4% efficiency.[1] This efficiency loss will scale up as devices become more efficient. The trend for Au behaves differently than Mo and Ti, in which both ρ_c and R_{sh} increase after annealing. The reason for this difference requires further investigation.

IV. CONCLUSIONS

In summary, the specific contact resistivities between Au, Mo, and Ti and SnS were investigated using TLM measurements. In a superstrate configuration, where the back

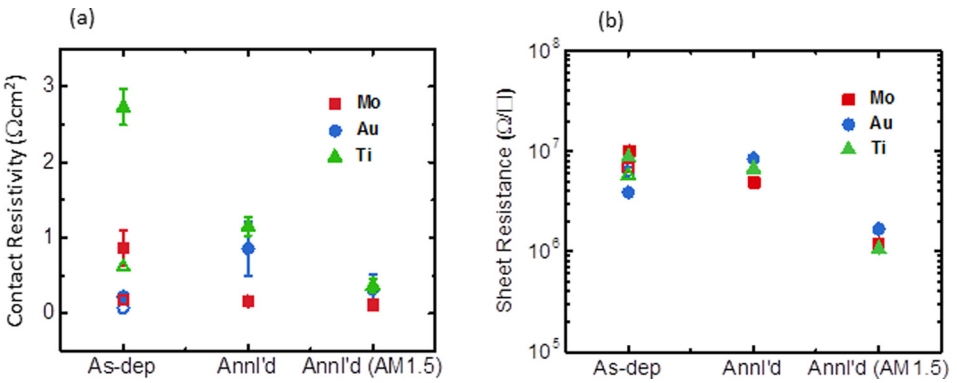

FIG. 4. (a) Contact resistivity at the metal-SnS interfaces and (b) SnS sheet resistance for as-deposited samples and H_2S-annealed samples measured both in dark and under AM1.5 light illumination. The filled symbols are for the substrate configuration, while the unfilled symbols for as-deposited samples represent values measured in the superstrate configuration.

metal contact is deposited on the SnS, the specific contact resistivities of Au/SnS, Mo/SnS, and Ti/SnS interfaces are 0.06 $\Omega\cdot cm^2$, 0.1 $\Omega\cdot cm^2$, and 0.6 $\Omega\cdot cm^2$, respectively. The Au and Mo back contacts have a satisfactorily low contact resistance for use in SnS solar cells. However, Ti back contacts would degrade the performance because of their high contact resistance with SnS. In the more commonly-used substrate configuration, the contact resistivities are all somewhat higher than in the superstrate configuration. Temperature-dependent TLM experiments demonstrated that the Fermi levels are strongly pinned, with barrier heights only ranging from 0.23 eV to 0.26 eV for the 3 metals tested. In the substrate structure, it was demonstrated that the contact resistance at the SnS/Mo and SnS/Ti interfaces decreased significantly after annealing the SnS film in an H_2S environment and further decreased when measured under AM 1.5 illumination. The contact resistivity at the back contact of the Mo substrate-based SnS solar cell is as low as 0.1 $\Omega\cdot cm^2$ under illumination. The efficiencies of current SnS solar cells are not significantly decreased by these contact resistances, although the effect would become more significant for cells with higher efficiency. This work provides information that is important for designing both substrate- and superstrate-based SnS solar cell devices. This approach also offers a framework for evaluating the quality of metal contacts to other emerging semiconductor materials.

SUPPLEMENTARY MATERIAL

See supplementary material for a cross-sectional SEM image of SnS on Mo/SiO_2 and X-ray diffraction of SnS films grown on Mo, Au, and Ti substrates.

ACKNOWLEDGMENTS

The authors thank Jason Tresback at Center for Nanoscale Systems (CNS) for his help with temperature dependent *I-V* measurement. This work was performed in part at the CNS, a member of the National Nanotechnology Coordinated Infrastructure Network (NNCI), which is supported by the National Science Foundation under NSF Award No. 1541959. CNS is part of Harvard University.

[1]P. Sinsermsuksakul, L. Sun, S. W. Lee, H. H. Park, S. B. Kim, C. Yang, and R. G. Gordon, Adv. Energy Mater. **4**, 1400496 (2014).
[2]V. Steinmann, R. Jaramillo, K. Hartman, R. Chakraborty, R. E. Brandt, J. R. Poindexter, Y. S. Lee, L. Sun, A. Polizzotti, and H. H. Park, Adv. Mater. **26**, 7488 (2014).
[3]J. Vidal, S. Lany, M. d'Avezac, A. Zunger, A. Zakutayev, J. Francis, and J. Tate, Appl. Phys. Lett. **100**, 032104 (2012).
[4]K. R. Reddy, N. K. Reddy, and R. Miles, Sol. Energy Mater. Sol. Cells **90**, 3041 (2006).
[5]N. M. Mangan, R. E. Brandt, V. Steinmann, R. Jaramillo, C. Yang, J. R. Poindexter, R. Chakraborty, H. H. Park, X. Zhao, and R. G. Gordon, J. Appl. Phys. **118**, 115102 (2015).
[6]S. Ashour and S. Alkuhaimi, Thin Solid Films **226**, 129 (1993).
[7]R. Jaramillo, M.-J. Sher, B. K. Ofori-Okai, V. Steinmann, C. Yang, K. Hartman, K. A. Nelson, A. M. Lindenberg, R. G. Gordon, and T. Buonassisi, J. Appl. Phys. **119**, 035101 (2016).
[8]W. M. Haynes, *CRC Handbook of Chemistry and Physics* (CRC Press, 2013).
[9]W. F. Gale and T. C. Totemeier, *Smithells Metals Reference Book* (Butterworth-Heinemann, 2003).
[10]R. Scheer and H.-W. Schock, *Chalcogenide Photovoltaics: Physics, Technologies, and Thin Film Devices* (John Wiley & Sons, 2011).
[11]K.-J. Yang, J.-H. Sim, B. Jeon, D.-H. Son, D.-H. Kim, S.-J. Sung, D.-K. Hwang, S. Song, D. B. Khadka, J. Kim, and J.-K. Kang, Prog. Photovoltaics Res. Appl. **23**, 862 (2014).
[12]R. Jaramillo, V. Steinmann, C. Yang, K. Hartman, R. Chakraborty, J. R. Poindexter, M. L. Castillo, R. Gordon, and T. Buonassisi, J. Visualized Exp. **22**, e52705 (2015).
[13]E. H. Rhoderick and R. H. Williams, *Metal-Semiconductor Contacts* (Clarendon Press Oxford, 1988).
[14]S. M. Sze and K. K. Ng, *Physics of Semiconductor Devices* (John wiley & sons, 2006).
[15]H. S. Yang, Y. Li, D. Norton, K. Ip, S. Pearton, S. Jang, and F. Ren, Appl. Phys. Lett. **86**, 192103 (2005).
[16]M. Devika, N. K. Reddy, F. Patolsky, and K. Gunasekhar, J. Appl. Phys. **104**, 124503 (2008).
[17]A. Andreev, M. Rastegaeva, V. Rastegaev, and S. Reshanov, Semiconductors **32**, 739 (1998).
[18]V. Stevanović, K. Hartman, R. Jaramillo, S. Ramanathan, T. Buonassisi, and P. Graf, Appl. Phys. Lett. **104**, 211603 (2014).
[19]E. Parthé and L. Gmelin, *Gmelin Handbook of Inorganic and Organometallic Chemistry: TYPIX. Standardized Data and Crystal Chemical Characterization of Inorganic Structure Types* (Springer, 1993).
[20]F. A. Padovani and R. Stratton, Solid State Electron. **9**, 695 (1966).
[21]S. Kurtin, T. McGill, and C. Mead, Phys. Rev. Lett. **22**, 1433 (1969).
[22]D. Avellaneda, M. Nair, and P. Nair, Thin Solid Films **517**, 2500 (2009).
[23]A. Schneikart, H. Schimper, A. Klein, and W. Jaegermann, J. Phys. D: Appl. Phys. **46**, 305109 (2013).
[24]W. Mönch, *Electronic Structure of Metal-Semiconductor Contacts* (Springer, 1990), pp. 224.
[25]R. Banai, L. Burton, S. Choi, F. Hofherr, T. Sorgenfrei, A. Walsh, B. To, A. Cröll, and J. Brownson, J. Appl. Phys. **116**, 013511 (2014).
[26]B. D. Malone, A. Gali, and E. Kaxiras, Phys. Chem. Chem. Phys. **16**, 26176 (2014).